

Ma, C., Foster, D.A., Mueller, P.A., Dutrow, B.L., and Marsh, J., 2020, Mesozoic crustal melting and metamorphism in the U.S. Cordilleran hinterland: Insights from the Sawtooth metamorphic complex, central Idaho: GSA Bulletin, <https://doi.org/10.1130/B35837.1>.

Supplemental Material

Figure S1. Geologic map of the Sawtooth metamorphic complex showing sample locations.

Figure S2. Photographs of outcrops from which the samples were collected.

Figure S3. Whole-rock trace elements of representative intrusive rocks shown as primitive-mantle-normalized spider diagrams.

Figure S4. Representative zircon trace elements plotted against individual zircon ages for intrusive rocks.

Figure S5. Chondrite-normalized rare earth elements of igneous zircons.

Appendix. Analytical Methods

Table S1. Sample location and lithology. (see the Excel file)

Table S2. Whole-rock major and trace elements. (see the Excel file)

Table S3. Zircon U-Pb data. (see the Excel file)

Table S4. Titanite U-Pb and trace element data. (see the Excel file)

Table S5. Zircon trace element data. (see the Excel file)

Table S6. Zircon Lu-Hf data. (see the Excel file)

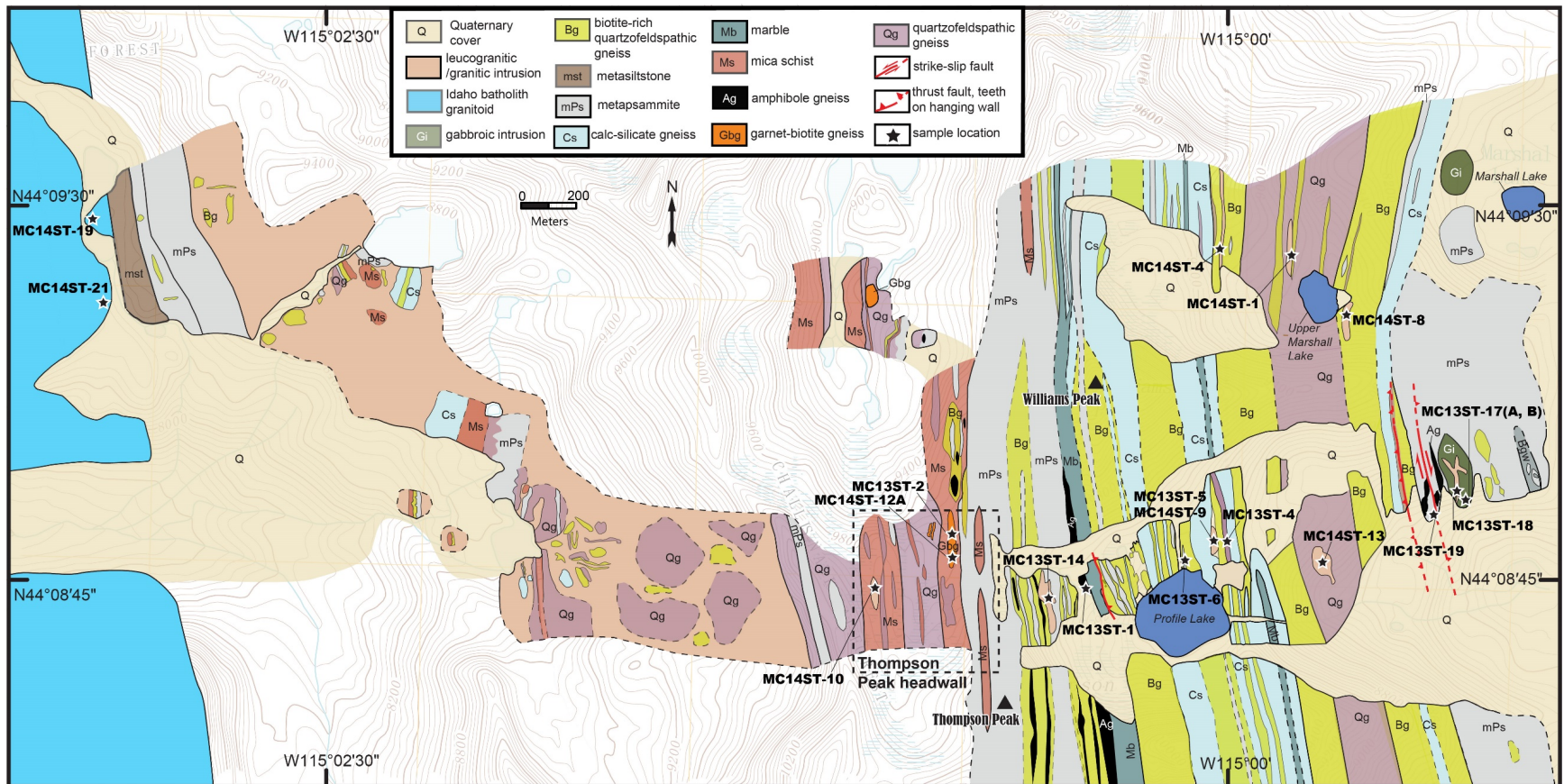


Figure S1. Geologic map of the Sawtooth metamorphic complex (Ma et al., 2017) showing sample locations. See location in Figure 1.

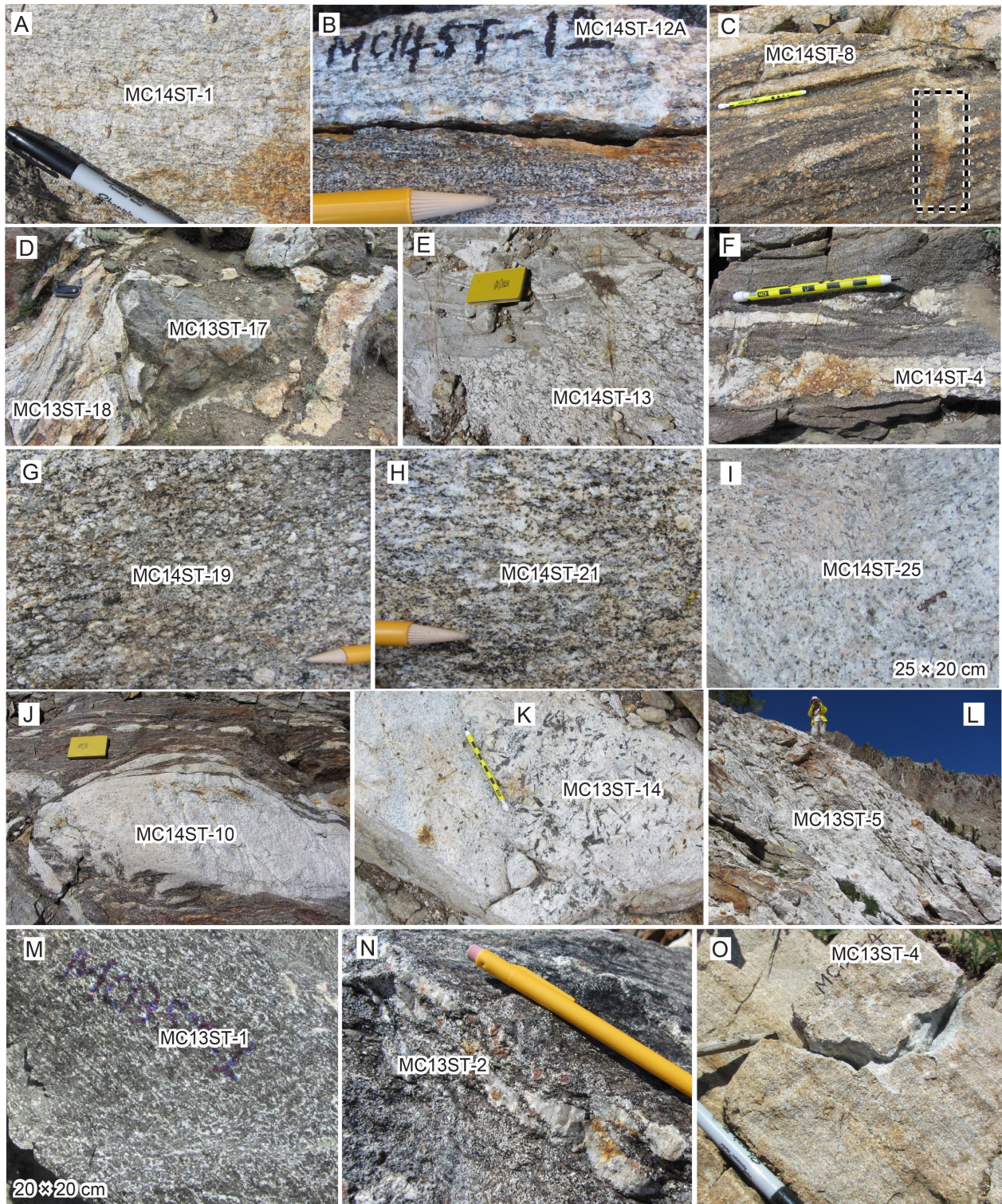


Figure S2. Photographs of outcrops from which the samples were collected. Detailed descriptions are provided in the text. Pen, person, notebook, and compass for scales. The dashed box in (C) highlights a felsic vein in the granitoid. Picture in (K) from Ma et al. (2017).

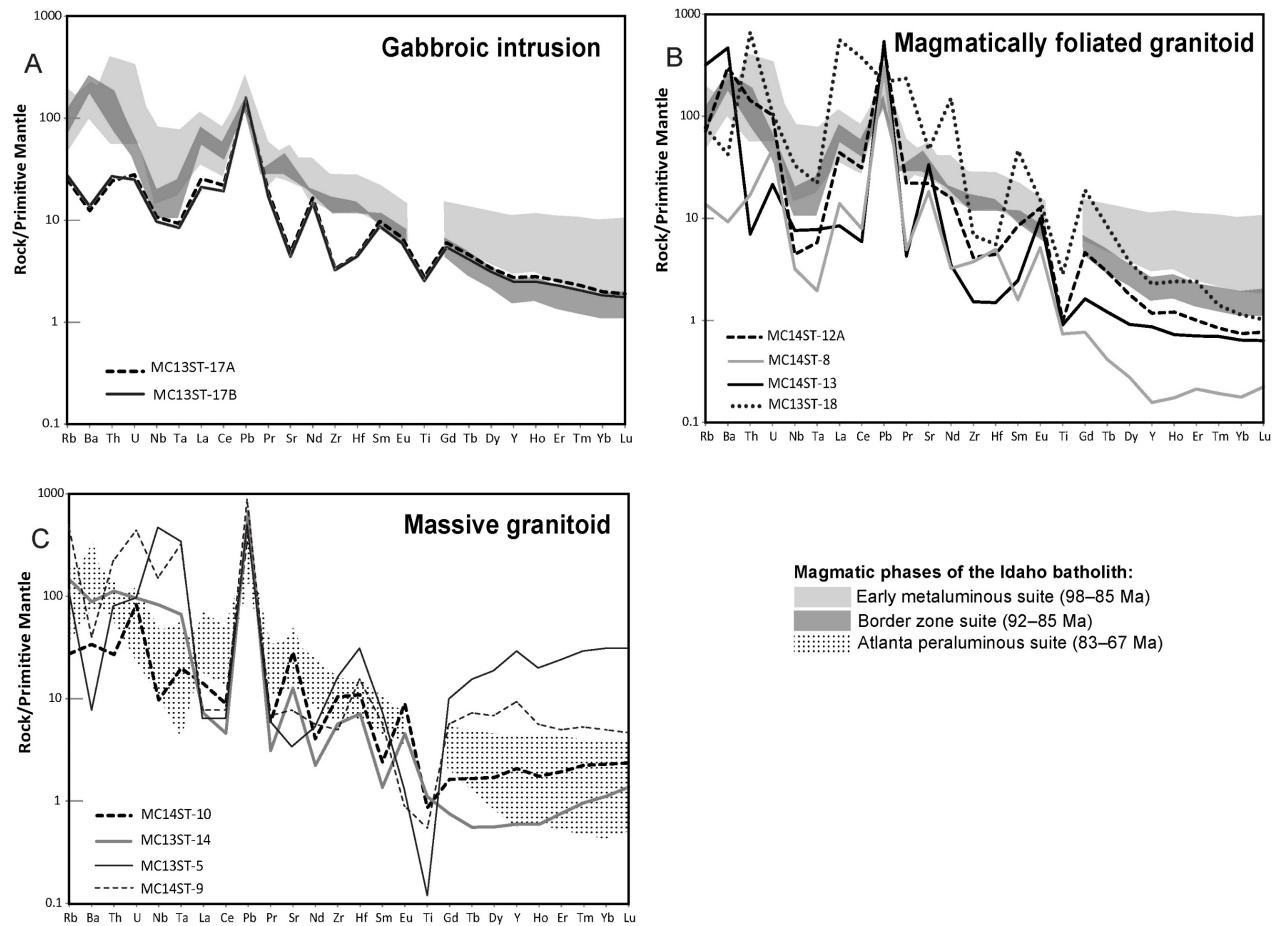


Figure S3. Whole-rock trace elements of representative intrusive rocks shown as primitive-mantle-normalized spider diagrams. Normalizing values are from Sun and McDonough (1989). Trace element data from three magmatic phases of the Idaho batholith (Gaschnig et al., 2011) are shown for comparison.

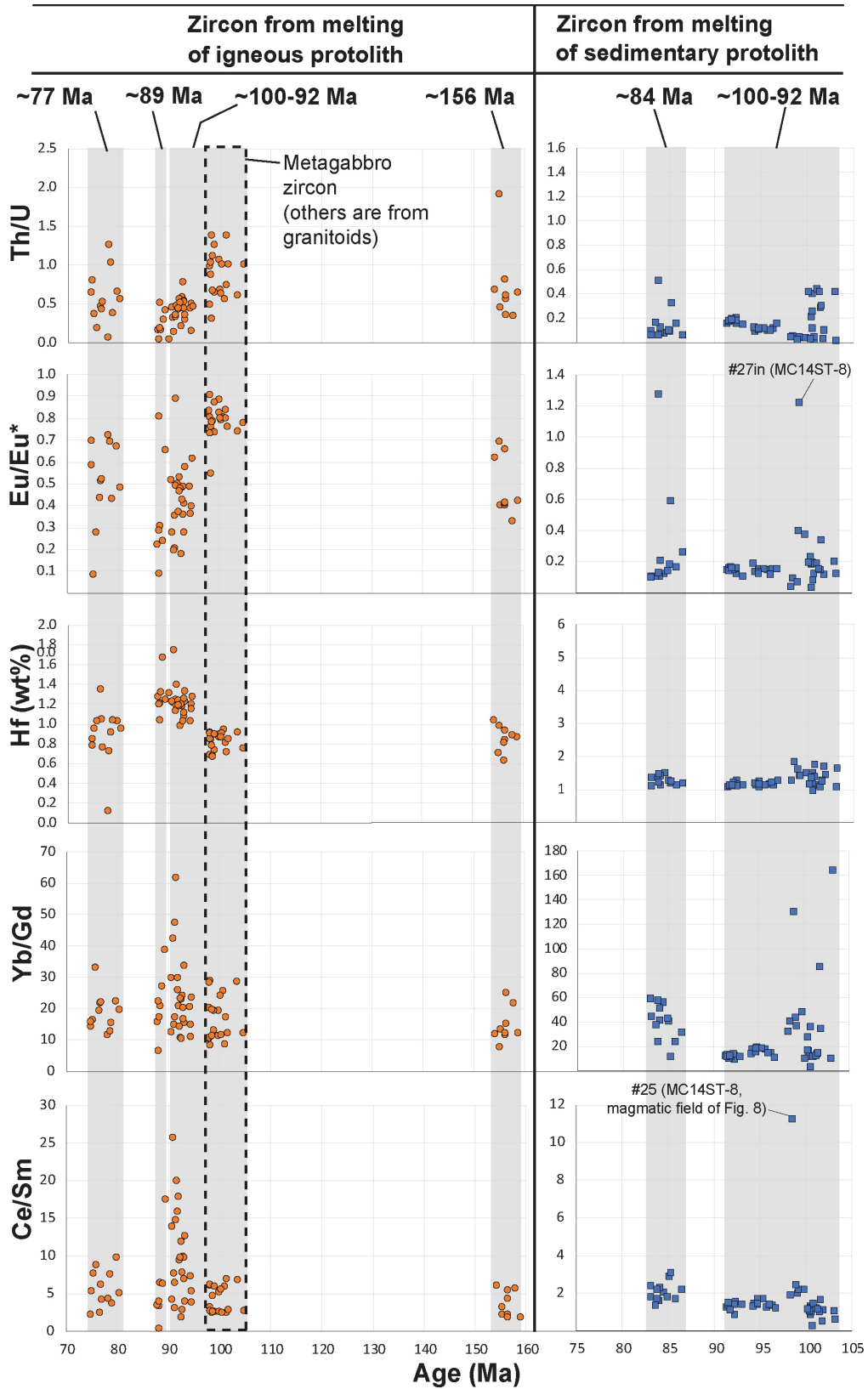


Figure S4. Representative zircon trace elements plotted against individual zircon ages for intrusive rocks.

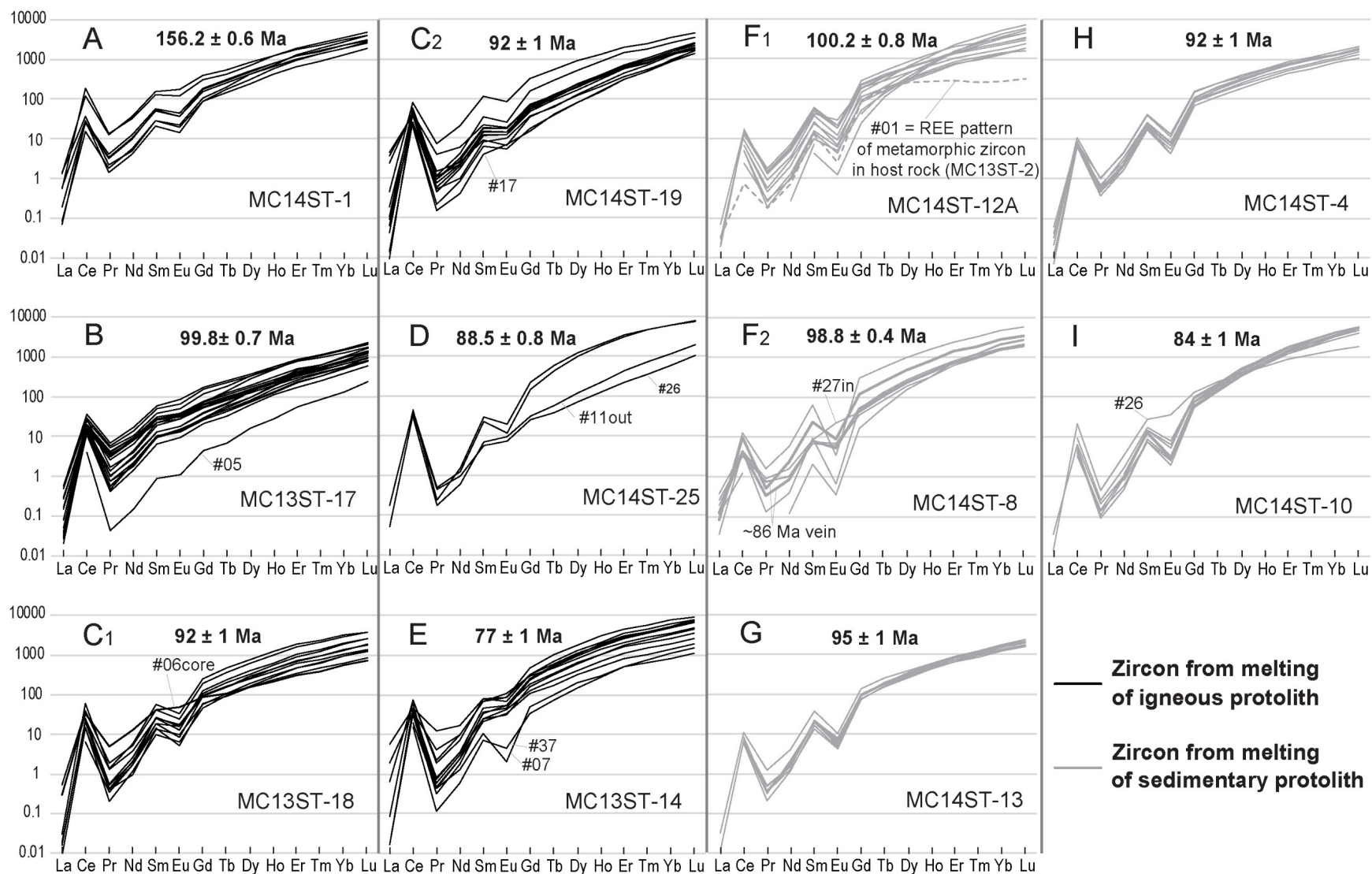


Figure S5. Chondrite-normalized rare earth elements of igneous zircons. The normalizing values are from McDonough and Sun (1995).

SUPPLEMENTARY APPENDIX: ANALYTICAL METHODS

Whole-Rock Major and Trace Elements

Whole-rock analyses were performed at the Department of Geological Sciences of the University of Florida. Fresh samples were carefully selected from outcrops and trimmed to be devoid of veins and alteration. Rock powders of each sample were baked overnight at ~ 110 °C to remove surface moisture. Two to 2.5 g of dried rock powder was left in a muffle furnace at ~ 950 °C for one hour. Loss on ignition was calculated by dividing the difference of the powder weight before and after heating. For making glass beads, 1.400 ± 0.005 g of dry rock powder was mixed with 5.600 ± 0.005 g of dry fusion flux (lithium borate), and fused at ~ 1200 °C with a Katanax K2 fluxer. Glass beads were analyzed on a Rigaku Supermini Wavelength Dispersive X-Ray Fluorescence spectrometer with United States Geological Survey standards AGV-1, BCR-1, and RGM-1 calibrating individual runs to the master standard file.

For trace element analyses, ~ 50 mg of finely ground rock powder was added to 2.5 ml purified (optima grade) concentrated HF in sealed PFA vials and left in an oven at 105 °C for >100 h. One ml concentrated HNO₃ (optima grade) was added to each capped vial and left in the oven for 24 hours, which was followed by drying on a hot plate to evaporate the liquid. Three ml of 6N ultrapure HCL was added to each of the dried samples and kept at 105 °C for at least 24 h. The next day, a small aliquot (~ 0.1 ml) of the sample solution was mixed with 3 ml 5% HNO₃ containing 8 ppb each of Re and Rh. The solution was analyzed on an Element2 Inductively Coupled Plasma-Mass Spectrometry with Re and Rh used as internal standards. Quantification of the results was done by external calibration using United States Geological Survey standards AGV-1 and RGM-1. See Kamenov et al. (2009) for more details.

Zircon U-Pb Geochronology

Zircon U-Pb analysis was also performed at the Department of Geological Sciences of the University of Florida. Samples were trimmed free of veins and alteration, then were crushed, milled, and sieved prior to zircon separation using magnetic and density-based methods followed by handpicking under a binocular microscope. The zircon grains were mounted in epoxy and polished. The grains were then imaged using cathodoluminescence and backscattered electrons to identify internal structures and compositional variations of the zircon. U-Pb isotopic analyses were performed on a Nu-Plasma multi-collector inductively coupled plasma mass spectrometer integrated with a New Wave 213 nm ultraviolet Nd:YAG laser ablation system following Mueller et al. (2008). Each analysis was carried out with a beam diameter of ~ 20 μm , and consists of a 20-second background measurement, 30-second ablation measurement, and a one-minute purging period. Zircons from the Duluth Gabbro Complex with an age of 1099.0 ± 0.6 Ma (FC-1; Paces and Miller, 1993; Black et al., 2003; Mattinson, 2010) were used as the age-reference for data calibration and drift correction. Data were reduced using an in-house Excel spreadsheet (CALAMARI) and plotted using Isoplot (Ludwig, 2012). When the TuffZirc algorithm (Ludwig and Mundil, 2002) is used, the single-grain dates older than the best estimate of crystallization age are interpreted to reflect data biased by older material. The younger dates are attributed to analyses biased by zircon overgrowth or subtle Pb loss. The coherent data identified by the TuffZirc algorithm may yield a linear array forming a regression line on a Tera-Wasserburg diagram, which gives the initial non-radiogenic Pb isotopic composition at the y-axis

intercept and true age at the lower intercept with the concordia curve, assuming a single initial or common Pb composition (Ludwig, 1998). If the coherent analyses used to define the median age do not statistically fit a line, Pb loss and/or mixing of multiple age domains likely affected the zircon (Schoene, 2014).

The U-Pb isotopic data reported in this study are $^{206}\text{Pb}/^{238}\text{U}$ ages for zircons younger than 1.0 Ga (only including data with <5% and >-3% discordance for magmatic zircon and data with <5% discordance for detrital zircon based on $^{206}\text{Pb}/^{238}\text{U}$ versus $^{207}\text{Pb}/^{235}\text{U}$), and $^{207}\text{Pb}/^{206}\text{Pb}$ ages for zircon older than 1.0 Ga (only including data with less than 10% discordance based on $^{206}\text{Pb}/^{238}\text{U}$ versus $^{207}\text{Pb}/^{206}\text{Pb}$). All analyses on the same grain were included in the results if they were different beyond two sigma errors; otherwise only the analyses with lower discordance were used.

Titanite U-Pb Geochronology

U-Pb isotope analyses of titanite were conducted by LA-ICP-MS at the Mineral Exploration Research Centre – Isotope Geochemistry Lab, at Laurentian University, Canada. Titanite grains were hand-picked under a binocular microscope, mounted in epoxy, and then polished. Titanites were imaged using backscattered electrons to identify internal structures and inclusions. Laser ablation sampling was performed using a Photon Machines Analyte G2 ArF excimer laser, with 193 nm wavelength, <4 ns pulse width, and HelEx II cell. Helium carrier gas flows through the ablation cell were for 0.525 l/min (cup) and 0.1 l/min (cell), with 0.65 l/min Ar and 6 ml/min N₂ makeup gas added downstream of the cell. Ablation spot diameter of 40 μm, laser fluence of 4 J/cm², and 7 Hz repetition rate were used. Ablation durations were 30 seconds, leaving estimated ablation pit depths of 15 μm. Sixty seconds of background were measured at the beginning and end of the analytical session, with 30 seconds of background measured between each ablation. The masses ^{88}r , ^{91}Zr , ^{204}Pb , ^{206}Pb , ^{207}Pb , ^{208}Pb , ^{232}Th , ^{238}U were measured on an iCap-TQ (quadrupole ICP-MS). Cool gas, auxiliary gas, and RF power were set at 14 L/min, 0.8 L/min, and 1550 W, respectively. During tuning on NIST612 synthetic glass prior to analysis the mean thorium oxide percent ($(^{248}\text{ThO}/^{232}\text{Th}) * 100$) was 0.65%. Extraction lens and Q1 entry lens voltages were tuned to maximize sensitivity in the high mass range.

The raw U-Pb data were processed in Iolite v3.6, with baseline subtraction, instrumental drift, and downhole fractionation corrections performed with the VizualAge data reduction scheme (Petrus and Kamber, 2012). The Khan titanite (522 ± 2.2 Ma; Heaman, 2009) was used as the primary reference material (RM) to normalize U-Pb isotope ratios and model downhole fractionation. The TCB titanite (1018.1 ± 1.7 Ma; Kennedy et al., 2010) was used as the secondary RM. Primary RM was analyzed three times at the beginning and end of each session, and once every ten unknown analyses throughout the session. Three seconds at the beginning and one second at end of each ablation period were excluded from the selections in order to minimize potential fractionation effects, leaving ~26 seconds of signal for integration. Ablation signals were inspected visually, with integration periods refined to exclude portions of the analyses with anomalously high ^{204}Pb or irregular $^{206}\text{Pb}/^{238}\text{U}$ age spectra. Within-run variance in the measured ratios for primary RM (i.e., the additional percent error required to achieve MSWD = 1) was propagated into the 2SE (standard error) uncertainty for all unknowns. A secondary RM was analyzed during each session to ensure accuracy of the U-Pb ratios and Zr concentrations, which yielded a concordia age of 1027 ± 9 Ma, similar to the 1018.1 ± 1.7 Ma of Kennedy et al. (2010) within error.

Zircon Trace Elements

Zircon trace element analyses were also conducted at the Mineral Exploration Research Centre – Isotope Geochemistry Lab at Laurentian University. Laser ablation (one spot per grain) sampling was performed using a Photon Machines Analyte G2 ArF excimer laser, with 193 nm wavelength, <4 ns pulse width, and HelEx II cell. Helium carrier gas flows through the ablation cell were for 0.65 l/min (cup) and 0.15 l/min (cell), with 0.725 l/min Ar and 6 ml/min N₂ makeup gas added downstream of the cell. Ablation spot diameter of 25 µm, laser fluence of 2 J/cm², and 7 Hz repetition rate were used. Ablation durations were 30 seconds, leaving estimated ablation pit depths of 15 µm. Sixty seconds of background were measured at the beginning and end of the analytical session, with 30 seconds of background measured between each ablation. The trace elements were measured on an iCap-TQ (quadrupole ICP-MS) with various dwell times: Si, Ca, Zr, Hf = 5 ms; P, Sc, Sr, Y, Nb, Ce, Tb, Dy, Ho, Er, Tm, Yb, Lu, Ta, Th, U = 10 ms; Gd = 15 ms; Nd, Sm, Eu = 25 ms; Pr = 50 ms; and Ti, La = 90 ms. Cool gas, auxiliary gas, and RF power were set at 14 L/min, 0.8 L/min, and 1550 W, respectively. During tuning on NIST612 synthetic glass prior to analysis the mean thorium oxide percent ($(^{248}\text{ThO}/^{232}\text{Th}) \cdot 100$) was 0.72%. Extraction lens and Q1 entry lens voltages were tuned to maximize sensitivity in the high mass range.

The raw data were processed in Iolite v3.6, with baseline subtraction, instrumental drift, and mass bias corrections performed with the Trace Element – Internal Standard data reduction scheme. The primary reference material (NIST610) was analyzed three times at the beginning and end of the session, and once every ten unknown analyses throughout the session. Three seconds at the beginning and one second at end of each ablation period were excluded from the selections in order to minimize potential fractionation effects, leaving ~26 seconds of signal for integration. Ablation signals were inspected visually, with integration periods refined to exclude irregular portions of the signal. Two secondary reference materials (NIST612 and 91500) were analyzed during the session to ensure accuracy of the concentrations, with values of 39.1 and 587 ppm zirconium, respectively.

Zircon Lu-Hf Isotopes

Zircon Lu-Hf analysis was performed at the Department of Geological Sciences of the University of Florida. Zircons analyzed for Lu-Hf were chosen based on their U-Pb ages and associated discordance, grain size, and zonation features revealed by cathodoluminescence images. Lu-Hf isotopic analyses were performed on the same Nu-Plasma multi-collector inductively coupled plasma mass spectrometer system that used for the U-Pb analyses. Each analysis was carried out with a beam diameter of ~40 µm, and consisted of a 20-second background measurement, one-minute ablation measurement, and a one-minute purging period. Methods of Hf isotopic measurements, Lu and Yb isobaric interference corrections, and mass-bias corrections are following Mueller et al. (2008). The analyses were calibrated with the reference zircon FC-1 that has a $^{176}\text{Hf}/^{177}\text{Hf}$ ratio of 0.28217 (± 0.00003 , 2σ) (Mueller et al., 2008; Foster et al., 2012). Initial $^{176}\text{Hf}/^{177}\text{Hf}$ values are calculated on the basis of measured and mass-bias corrected $^{176}\text{Lu}/^{177}\text{Hf}$ ratios of individual zircon and the crystallization age (obtained separately by U-Pb dating of the same zircon) of the associated sample. ϵ_{Hf} values are calculated based on the CHUR values of Bouvier et al. (2008). Depleted mantle values are after the linear

model ($\epsilon_{\text{Hf}} = 0$ at 4.56 Ga and 16 at 0 Ga) of Mueller et al. (2008). The ^{176}Lu decay constant ($1.867 \times 10^{-11} \text{ yr}^{-1}$) is after Söderlund et al. (2004).

Whole-Rock Sm-Nd Isotopes

Whole-rock Sm-Nd analysis was also conducted at the Department of Geological Sciences of the University of Florida. Sm-Nd isotopes were separated using standard chromatographic methods in a class 500 clean lab. Neodymium isotopic compositions were measured on a Nu-Plasma multi-collector inductively coupled plasma mass spectrometer following Kamenov et al. (2008). In brief, analyte ions were placed in small volume and the whole sample was aspirated in the plasma through a DSN-100 desolvating nebulizer. The Nu-Plasma “Time-Resolved Analysis” software was used to select data and was operating with 0.2 s integration time to get acquisition of 300 ratios per minute. Nd isotopic ratios were measured in static mode acquiring simultaneously ^{142}Nd on low-2, ^{143}Nd on low-1, ^{144}Nd on Axial, ^{145}Nd on high-1, ^{146}Nd on high-2, ^{147}Sm on high-3, ^{148}Nd on high-4, and ^{150}Nd on high-5 Faraday detectors. Isobaric interference of Sm was corrected for the measured ^{144}Nd , ^{148}Nd , and ^{150}Nd by applying $^{147}\text{Sm}/^{144}\text{Sm} = 4.88$, $^{147}\text{Sm}/^{144}\text{Sm} = 1.33$, $^{147}\text{Sm}/^{144}\text{Sm} = 2.03$. Using an exponential law for mass-bias correction, all measured ratios were normalized to $^{146}\text{Nd}/^{144}\text{Nd} = 0.7219$. Baseline was measured by electrostatic analyzer deflection of the beam. The Jndi-1 standard was analyzed three times during each session and yielded a mean value of 0.51212 ± 0.00002 (2σ error).

REFERENCES CITED

- Black, L.P., Kamo, S.L., Williams, I.S., Mundil, R., Davis, D.W., Korsch, R.J., and Foudoulis, C., 2003, The application of SHRIMP to Phanerozoic geochronology; a critical appraisal of four zircon standards: *Chemical Geology*, v. 200, no. 1–2, p. 171–188, [https://doi.org/10.1016/S0009-2541\(03\)00166-9](https://doi.org/10.1016/S0009-2541(03)00166-9).
- Bouvier, A., Vervoort, J.D., and Patchett, P.J., 2008, The Lu–Hf and Sm–Nd isotopic composition of CHUR: constraints from unequilibrated chondrites and implications for the bulk composition of terrestrial planets: *Earth and Planetary Science Letters*, v. 273, no. 1–2, p. 48–57, <https://doi.org/10.1016/j.epsl.2008.06.010>.
- Foster, D.A., Mueller, P.A., Heatherington, A., Gifford, J.N., and Kalakay, T.J., 2012, Lu–Hf systematics of magmatic zircons reveal a Proterozoic crustal boundary under the Cretaceous Pioneer batholith, Montana: *Lithos*, v. 142, p. 216–225, <https://doi.org/10.1016/j.lithos.2012.03.005>.
- Gaschnig, R.M., Vervoort, J.D., Lewis, R.S., and Tikoff, B., 2011, Isotopic evolution of the Idaho batholith and Challis intrusive province, northern US Cordillera: *Journal of Petrology*, v. 52, no. 12, p. 2397–2429, <https://doi.org/10.1093/petrology/egr050>.
- Heaman, L.M., 2009, The application of U–Pb geochronology to mafic, ultramafic and alkaline rocks: an evaluation of three mineral standards: *Chemical Geology*, v. 261, p. 43–52, <https://doi.org/10.1016/j.chemgeo.2008.10.021>.
- Kamenov, G.D., Brenner, M., and Tucker, J.L., 2009, Anthropogenic versus natural control on trace element and Sr–Nd–Pb isotope stratigraphy in peat sediments of southeast Florida (USA), 1500 AD to present: *Geochimica et Cosmochimica Acta*, v. 73, no. 12, p. 3549–3567, <https://doi.org/10.1016/j.gca.2009.03.017>.

- Kamenov, G.D., Perfit, M.R., Mueller, P.A., and Jonasson, I.R., 2008, Controls on magmatism in an island arc environment: study of lavas and sub-arc xenoliths from the Tabar–Lihir–Tanga–Feni island chain, Papua New Guinea: *Contributions to Mineralogy and Petrology*, v. 155, no. 5, p. 635–656, <https://doi.org/10.1007/s00410-007-0262-0>.
- Kennedy, A.K., Kamo, S.L., Nasdala, L., and Timms, N.E., 2010, Grenville skarn titanite: potential reference material for SIMS U–Th–Pb analysis: *Canadian Mineralogist*, v. 48, p. 1423–1443, <https://doi.org/10.3749/canmin.48.5.1423>.
- Ludwig, K.R., 1998, On the treatment of concordant uranium-lead ages: *Geochimica et Cosmochimica Acta*, v. 62, no. 4, p. 665–676, [https://doi.org/10.1016/S0016-7037\(98\)00059-3](https://doi.org/10.1016/S0016-7037(98)00059-3).
- Ludwig, K.R., 2012, User’s manual for Isoplot 3.75: A geochronological toolkit for Microsoft Excel: Berkeley Geochronology Center Special Publication No. 5, 75 p.
- Ludwig, K.R., and Mundil, R., 2002, Extracting reliable U–Pb ages and errors from complex populations of zircons from Phanerozoic tuffs: *Geochimica et Cosmochimica Acta*, v. 66, p. 463.
- Ma, C., Foster, D.A., Mueller, P.A., and Dutrow, B.L., 2017, Magma-facilitated transpressional strain partitioning within the Sawtooth metamorphic complex, Idaho: A zone accommodating Cretaceous orogen-parallel translation in the Idaho batholith: *Tectonics*, v. 36, no. 3, p. 444–465, <https://doi.org/10.1002/2016TC004264>.
- Mattinson, J.M., 2010, Analysis of the relative decay constants of ^{235}U and ^{238}U by multi-step CA- TIMS measurements of closed-system natural zircon samples: *Chemical Geology*, v. 275, no. 3–4, p. 186–198, <https://doi.org/10.1016/j.chemgeo.2010.05.007>.
- McDonough, W.F., and Sun, S.S., 1995, The composition of the Earth: *Chemical Geology*, v. 120, p. 223–253, [https://doi.org/10.1016/0009-2541\(94\)00140-4](https://doi.org/10.1016/0009-2541(94)00140-4).
- Mueller, P.A., Kamenov, G.D., Heatherington, A.L., and Richards, J., 2008, Crustal evolution in the southern Appalachian orogen: Evidence from Hf isotopes in detrital zircons: *The Journal of Geology*, v. 116, no. 4, p. 414–422, <https://doi.org/10.1086/589311>.
- Paces, J.B., and Miller, J.D., 1993, Precise U–Pb ages of Duluth Complex and related mafic intrusions, northeastern Minnesota: Geochronological insights to physical, petrogenetic, paleomagnetic, and tectonomagmatic processes associated with the 1.1 Ga Midcontinent Rift System: *Journal of Geophysical Research*, v. 98, no. B8, p. 13997–14013, <https://doi.org/10.1029/93JB01159>.
- Petrus, J.A., and Kamber, B.S., 2012, VizualAge: A Novel Approach to Laser Ablation ICP-MS U–Pb Geochronology Data Reduction: *Geostandards and Geoanalytical Research*, v. 36, p. 247–270, <https://doi.org/10.1111/j.1751-908X.2012.00158.x>.
- Schoene, B., 2014, U–Th–Pb Geochronology: *Treatise on Geochemistry*, v. 4, p. 341–378, <https://doi.org/10.1016/B978-0-08-095975-7.00310-7>.
- Söderlund, U., Patchett, P.J., Vervoort, J.D., and Isachsen, C.E., 2004, The ^{176}Lu decay constant determined by Lu–Hf and U–Pb isotope systematics of Precambrian mafic intrusions: *Earth and Planetary Science Letters*, v. 219, p. 311–324, [https://doi.org/10.1016/S0012-821X\(04\)00012-3](https://doi.org/10.1016/S0012-821X(04)00012-3).
- Sun, S.S., and McDonough, W.F., 1989, Chemical and isotopic systematics of oceanic basalts: implications for mantle composition and processes, *in* Saunders, A.D., and Norry, M.J., eds., *Magmatism in ocean basins*: Geological Society, London, Special Publications, v. 42, p. 313–345, <https://doi.org/10.1144/GSL.SP.1989.042.01.19>.